

Flexible Neural Representation for Physics Prediction

Damian Mrowca*
Stanford

Chengxu Zhuang*
Stanford

Elias Wang*
Stanford

Nick Haber
Stanford

Li Fei-Fei
Stanford

Joshua B. Tenenbaum
MIT

Daniel L. K. Yamins
Stanford

Abstract

Humans have a remarkable capacity to understand the physical dynamics of objects in their environment, flexibly capturing complex structures and interactions at multiple levels of detail. Inspired by this ability, we propose a hierarchical particle-based object representation that covers a wide variety of types of three-dimensional objects, including both arbitrary rigid geometrical shapes and deformable materials. We then describe the Hierarchical Relation Network (HRN), an end-to-end differentiable neural network based on hierarchical graph convolution, that learns to predict physical dynamics in this representation. Compared to other neural network baselines, the HRN accurately handles complex collisions and nonrigid deformations, generating plausible dynamics predictions at long time scales in novel settings, and scaling to large scene configurations. These results demonstrate an architecture with the potential to form the basis of next-generation physics predictors for use in computer vision, robotics, and quantitative cognitive science.

1 Introduction

Humans efficiently decompose their environment into objects, and reason effectively about the dynamic interactions between these objects [41, 43]. Although human intuitive physics may be quantitatively inaccurate under some circumstances [31], humans make qualitatively plausible guesses about dynamic trajectories of their environments over long time horizons [39]. Moreover, they are either born knowing, or quickly learn about, concepts such as object permanence, occlusion, and deformability, which guide their perception and reasoning [40].

An artificial system that could mimic such abilities would be of great use for applications in computer vision, robotics, reinforcement learning, and many other areas. While traditional physics engines constructed for computer graphics have made great strides, such routines are often hard-wired and thus challenging to integrate as components of larger learnable systems. Creating end-to-end differentiable neural networks for physics prediction is thus an appealing idea. Recently, Chang et al. [11] and Battaglia et al. [4] have illustrated the use of neural networks to predict physical object interactions in (mostly) 2D scenarios by proposing object-centric and relation-centric representations. Common to these works is the treatment of scenes as graphs, with nodes representing object point masses and edges describing the pairwise relations between objects (e.g. gravitational, spring-like, or repulsing relationships). Object relations and physical states are used to compute the pairwise effects between objects. After combining effects on an object, the future physical state of the environment is predicted on a per-object basis. This approach is very promising in its ability to explicitly handle object interactions. However, a number of challenges have remained in generalizing this approach to real-world physical dynamics, including representing arbitrary geometric shapes with sufficient

*equal contribution

resolution to capture complex collisions, working with objects at different scales simultaneously, and handling non-rigid objects of nontrivial complexity.

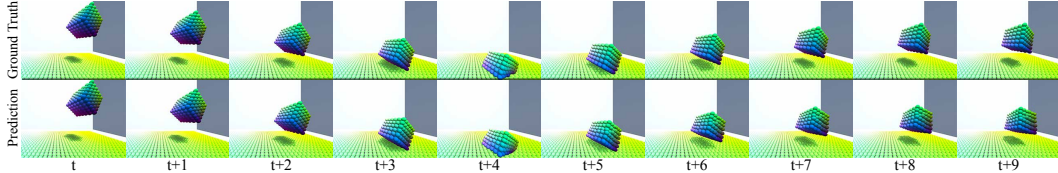


Figure 1: **Predicting physical dynamics.** Given past observations the task is to predict the future physical state of a system. In this example, a cube deforms as it collides with the ground. The top row shows the ground truth and the bottom row the prediction of our physics prediction network.

Several of these challenges are illustrated in the fast-moving deformable cube sequence depicted in Figure 1. Humans can flexibly vary the level of detail at which they perceive such objects in motion: The cube may naturally be conceived as an undifferentiated point mass as it moves along its initial kinematic trajectory. But as it collides with and bounces up from the floor, the cube’s complex rectilinear substructure and nonrigid material properties become important for understanding what happens and predicting future interactions. The ease with which the human mind handles such complex scenarios is an important explicandum of cognitive science, and also a key challenge for artificial intelligence. Motivated by both of these goals, our aim here is to develop a new class of neural network architectures with this human-like ability to reason flexibly about the physical world.

To this end, it would be natural to extend the interaction network framework by representing each object as a (potentially large) set of connected particles. In such a representation, individual constituent particles could move independently, allowing the object to deform while being constrained by pairwise relations preventing the object from falling apart. However, this type of particle-based representation introduces a number of challenges of its own. Conceptually, it is not immediately clear how to efficiently propagate effects across such an object. Moreover, representing every object with hundreds or thousands of particles would result in an exploding number of pairwise relations, which is both computationally infeasible and cognitively unnatural.

As a solution to these issues, we propose a novel cognitively-inspired hierarchical graph-based object representation that captures a wide variety of complex rigid and deformable bodies (Section 3), and an efficient hierarchical graph-convolutional neural network that learns physics prediction within this representation (Section 4). Evaluating on complex 3D scenarios, we show substantial improvements relative to strong baselines both in quantitative prediction accuracy and qualitative measures of prediction plausibility, and evidence for generalization to complex unseen scenarios (Section 5).

2 Related Work

An efficient and flexible predictor of physical dynamics has been an outstanding question in neural network design. In computer vision, modeling moving objects in images or videos for action recognition, future prediction, and object tracking is of great interest. Similarly in robotics, action-conditioned future prediction from images is crucial for navigation or object interactions. However, future predictors operating directly on 2D image representations often fail to generate sharp object boundaries and struggle with occlusions and remembering objects when they are no longer visually observable [1, 16, 15, 27, 28, 32, 33, 18]. Representations using 3D convolution or point clouds are better at maintaining object shape [44, 45, 10, 35, 36], but do not entirely capture object permanence, and can be computationally inefficient. More similar to our approach are inverse graphics methods that extract a lower dimensional physical representation from images that is used to predict physics [24, 25, 49, 48, 50, 51, 7, 47]. Our work draws inspiration from and extends that of Chang et al. [11] and Battaglia et al. [4], which in turn use ideas from graph-based neural networks [37, 42, 9, 29, 21, 14, 13, 23, 8, 38]. Most of the existing work, however, does not naturally handle complex scene scenarios with objects of widely varying scales or deformable objects with complex materials.

Physics simulation has also long been studied in computer graphics, most commonly for rigid-body collisions [2, 12]. Particles or point masses have also been used to represent more complex physical objects, with the neural network-based NeuroAnimator being one of the earliest examples to use a

hierarchical particle representation for objects to advance the movement of physical objects [17]. Our particle-based object representation also draws inspiration from recent work on (non-neural-network) physics simulation, in particular the NVIDIA FleX engine [30, 6]. However, unlike this work, our solution is an end-to-end differentiable neural network that can learn from data.

Recent research in computational cognitive science has posited that humans run physics simulations in their mind [5, 3, 19, 46, 20]. It seems plausible that such simulations happen at just the right level of detail which can be flexibly adapted as needed similar to our proposed representation. Both the ability to imagine object motion as well as to flexibly decompose an environment into objects and parts form an important prior that humans rely on for further learning about new tasks, when generalizing their skills to new environments or flexibly adapting to changes in inputs and goals [26].

3 Hierarchical Particle Graph Representation

A key factor for predicting the future physical state of a system is the underlying representation used. A simplifying, but restrictive, often made assumption is that all objects are rigid. A rigid body can be represented with a single point mass and unambiguously situated in space by specifying its position and orientation, together with a separate data structure describing the object’s shape and extent. Examples are 3D polygon meshes or various forms of 2D or 3D masks extracted from perceptual data [10, 15]. The rigid body assumption describes only a fraction of the real world, excluding e.g. soft bodies, fluids, and gases, and precludes objects breaking and combining. However, objects are divisible and made up of a potentially large numbers of smaller sub-parts.

Given a scene with a set of objects O , the core idea is to represent each object $o \in O$ with a set of particles $P_o \equiv \{p_i | i \in o\}$. Each particle is labeled with three pieces of relevant state information, including its position $x \in \mathbb{R}^3$, its velocity $\delta \in \mathbb{R}^3$, and mass $m \in \mathbb{R}^+$, and we refer to p_i and this vector in \mathbb{R}^7 interchangeably.

Particles are spaced out across an object to fully describe its volume. In theory particles can be arbitrarily placed within an object. Thus, less complex parts can be described with fewer particles (e.g. 8 particles fully define a cube). More complicated parts can be represented with more particles (e.g. a long rod). We define P as the set $\{p_i | 1 \leq i \leq N_P\}$ of all N_P particles in the observed scene.

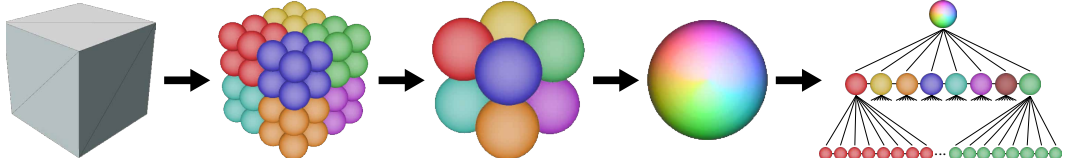


Figure 2: **Hierarchical graph-based object representation.** An object is decomposed into particles. Particles (of the same color) are grouped into a hierarchy representing multiple object scales. Pairwise relations constrain particles in the same group and to ancestors and descendants.

But particles alone are not enough to describe a scene containing multiple objects. We also need to describe how the particles relate to each other. Similar to Battaglia et al. [4], we use K -dimensional pairwise relationships $R = \{r_{ij} \in \mathbb{R}^K\}$ between particles p_i and p_j to represent this. However, in our representation, not all pairs of particles are related. Instead, pairs of particles within an object are related, while particles in different objects are not. Each relationship r_{ij} within the object encodes material property information, which we assume to depend only on the source particle p_i . In what follows, $K = 1$ and $r_{ij} \in \mathbb{R}$ represents the local stiffness of the material. Note that this interpretation is learned from data rather than hard-coded. We make no supposition that this value is uniform within an object. Arbitrarily-shaped objects in a wide variety of (potentially nonuniform) materials can be represented in this way. Overall, we represent the scene by a node-labeled graph $G = \langle P, R \rangle$ where the particles form the nodes P and the relations define the (directed) edges R . Different objects are disconnected components within G .

The graph G is used to propagate effects through the scene. It would be infeasible to use a fully connected graph for propagation as pairwise-relationship computations would grow with $\mathcal{O}(N_P^2)$. Thus, we construct a *hierarchical scene (di)graph* G_H from G where the nodes within each connected component are organized into a tree structure, so that dynamics calculations scale with $\mathcal{O}(N_P \log(N_P))$:

First, we initialize the leaf nodes L of G_H as the original particle set P . Then, we extend G_H by a root node for each connected component (object) in G . The root node states are defined as the aggregates of the leaf nodes states of the respective components. The root nodes are connected to their leaves with directed edges and vice versa.

At this point, G_H consists of the leaf particles L representing the finest scene resolution and one root node for each connected component describing the scene at the object level. To obtain intermediate levels of detail, we then cluster the leaves L in each connected component into smaller subcomponents using a modified k-means algorithm. We add one node for each new subcomponent and connect its leaves to the added node and vice versa. We then connect the added intermediate nodes with each other if and only if their respective subcomponent leaves are connected. Lastly, we add directed edges from the root node of each connected component to the new intermediate nodes in that component, and remove edges between leaves not in the same cluster. The process then recurses within each new subcomponent. See Algorithm 1 in the supplementary for details.

We denote the sibling(s) of a particle p by $\text{sib}(p)$, its ancestor(s) by $\text{anc}(p)$, its parent by $\text{par}(i)$, and its descendant(s) by $\text{des}(p)$. We define $\text{leaves}(p_a) = \{p_l \in L \mid p_a \in \text{anc}(p_l)\}$. Note that in G_H , directed edges remain only between p_i and $\text{sib}(p_i)$, leaves p_l and $\text{anc}(p_l)$, and p_i and $\text{des}(p_i)$, as seen in Figure 3 b).

4 Physics Prediction Model

In this section we introduce our physics prediction model. It is based on hierarchical graph convolution, an operation which propagates relevant physical effects through the graph hierarchy.

4.1 Hierarchical Graph Convolutions For Effect Propagation

In order to predict the future physical state, we need to resolve the constraints that particles connected in the hierarchical graph impose on each other. We use graph convolutions to compute and propagate these effects. Following Battaglia et al. [4], we implement a *pairwise graph convolution* using two basic building blocks: (1) A pairwise processing unit ϕ that takes the sender particle state p_s , the receiver particle state p_r and their relation r_{sr} as input and outputs the effect $e_{sr} \in \mathbb{R}^E$ of p_s on p_r , and (2) a commutative aggregation operation Σ which collects and computes the overall effect $e_r \in \mathbb{R}^E$. In our case this is a simple summation over all effects on p_r . Together these two building blocks form a convolution on graphs as shown in Figure 3 a).

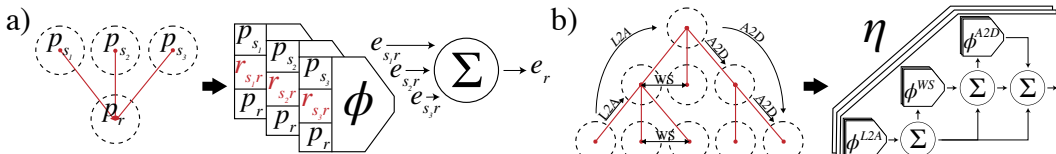


Figure 3: **Effect propagation through graph convolutions.** a) **Pairwise graph convolution ϕ .** A receiver particle p_r is constrained in its movement through graph relations r_{sr} with sender particle(s) p_s . Given p_s , p_r and r_{sr} , the effect e_{sr} of p_s on p_r is computed using a fully connected neural network. The overall effect e_r is the sum of all effects on p_r . b) **Hierarchical graph convolution η .** Effects in the hierarchy are propagated in three consecutive steps. (1) ϕ^{L2A} . Leaf particles L propagate effects to all of their ancestors A . (2) ϕ^{WS} . Effects are exchanged between siblings S . (3) ϕ^{A2D} . Effects are propagated from the ancestors A to all of their descendants D .

Pairwise processing limits graph convolutions to only propagate effects between directly connected nodes. For a generic graph, we would have to repeatedly apply this operation until the information from all particles has propagated across the whole graph. This is infeasible in a scenario with many particles. Instead, we leverage direct connections between particles and their ancestors in our hierarchy for faster propagation. We thus introduce a *hierarchical graph convolution*, a three stage mechanism for effect propagation (see Figure 3 b):

The first *L2A* (*Leaves to Ancestors*) stage $\phi^{L2A}(p_l, p_a, r_{la}, e_l^0)$ predicts the effect $e_{la}^{L2A} \in \mathbb{R}^E$ of a leaf particle p_l on an ancestor particle $p_a \in \text{anc}(p_l)$ given p_l , p_a , the material property information of r_{la} , and input effect e_l^0 on p_l . The second *WS* (*Within Siblings*) stage $\phi^{WS}(p_i, p_j, r_{ij}, e_i^{L2A})$

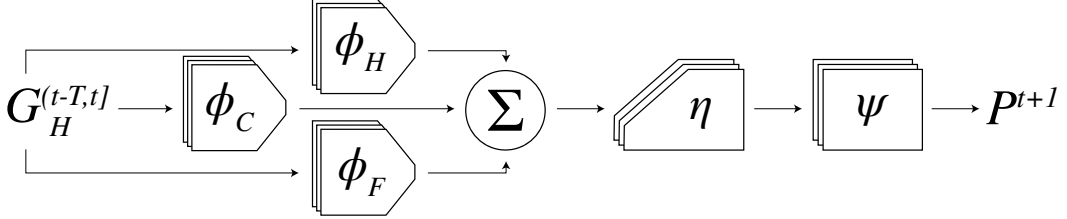


Figure 4: **Hierarchical Relation Network.** The model takes the past particle graphs $G_H^{(t-T,t]} = \langle P^{(t-T,t]}, R^{(t-T,t]}\rangle$ as input and outputs the next states P^{t+1} . The inputs to each graph convolutional effect module ϕ are the particle states and relations, the outputs the respective effects. ϕ_H processes past states, ϕ_C collisions, and ϕ_F external forces. The hierarchical graph convolutional module η takes the sum of all effects, the pairwise particle states, and relations and propagates the effects through the graph. Finally, ψ uses the propagated effects to compute the next particle states P^{t+1} .

predicts the effect $e_{ij}^{WS} \in \mathbb{R}^E$ of sibling particle p_i on $p_j \in \text{sib}(p_i)$. The third A2D (*Ancestors to Descendants*) stage $\phi^{A2D}(p_a, p_d, r_{ad}, e_a^{L2A} + e_a^{WS})$ predicts the effect $e_{ij}^{A2D} \in \mathbb{R}^E$ of an ancestor particle p_a on a descendant particle $p_d \in \text{des}(p_a)$. Effects for each particle are summed together.

All in all, the total propagated effect e_i on particle p_i then equals $e_i = e_i^{L2A} + e_i^{WS} + e_i^{A2D}$ where

$$e_a^{L2A} = \sum_{p_l \in \text{leaves}(p_a)} \phi^{L2A}(p_l, p_a, r_{la}, e_l^0) \quad e_j^{WS} = \sum_{p_i \in \text{sib}(p_j)} \phi^{WS}(p_i, p_j, r_{ij}, e_i^{L2A})$$

$$e_d^{A2D} = \sum_{p_a \in \text{anc}(p_d)} \phi^{A2D}(p_a, p_d, r_{ad}, e_a^{L2A} + e_a^{WS})$$

In practice, ϕ^{L2A} , ϕ^{WS} , and ϕ^{A2D} are implemented as fully-connected networks that receive an additional ternary input (0 for L2A, 1 for WS, and 2 for A2D) and share weights.

Since all particles are connected to the root node, information can flow across the entire hierarchical graph in at most two steps. We make use of this property in our physics prediction model.

4.2 The Hierarchical Relation Network Architecture

This section introduces the *Hierarchical Relation Network* (HRN), a neural network architecture for predicting future physical states shown in Figure 4. At each time step t , HRN takes a history of T previous particle states $P^{(t-T,t]}$ and relations $R^{(t-T,t]}$ in the form of hierarchical scene graphs $G_H^{(t-T,t]}$ as input. $G_H^{(t-T,t]}$ dynamically changes over time as undirected, unlabeled virtual collision relations are added for sufficiently close pairs of otherwise disconnected particles. HRN also takes external effects on the system (e.g. gravity g or external forces F) as input. The model consists of three pairwise graph convolution modules, one for external forces (ϕ_F), one for collisions (ϕ_C) and one for past states (ϕ_H), followed by a hierarchical graph convolution module η that propagates effects through the particle hierarchy. A fully-connected module ψ then outputs the next states P^{t+1} .

In the following, we briefly describe each module. For ease of reading we *drop the notation* $(t-T, t]$ and assume that all variables are subject to this time range unless otherwise noted.

External Force Module The *external force module* ϕ_F converts forces $F \equiv \{f_i\}$ on leaf particles $p_i \in P^L$ into effects $\phi_F(p_i, f_i) = e_i^F \in \mathbb{R}^E$.

Collision Module Collisions are handled by dynamically defining pairwise collision relations r_{ij}^C between leaf particles $p_i \in P^L$ and $p_j \in P^L$ that are close to each other [11]. The *collision module* ϕ_C uses p_i , p_j and r_{ij}^C to compute the effects $\phi_C(p_j, p_i, r_{ij}^C) = e_{ji}^C \in \mathbb{R}^E$ of p_j on p_i and vice versa. With $d^t(i, j) = \|x_i^t - x_j^t\|$, the overall collision effects equal $e_i^C = \sum_j \{e_{ji} | d^t(i, j) < D_C\}$. The hyperparameter D_C represents the maximum distance for a collision relation.

History Module The *history module* ϕ_H predicts the effects $\phi(p_i^{(t-T,t-1]}, p_i^t) \in e_i^H$ from past $p_i^{(t-T,t-1]} \in P^L$ on current leaf particle states $p_i^t \in P^L$.

Hierarchical Effect Propagation Module The *hierarchical effect propagation module* η propagates the overall effect $e_i^0 = e_i^F + e_i^C + e_i^H$ from external forces, collisions and history on p_i through the particle hierarchy. η corresponds to the three-stage hierarchical graph convolution introduced in Figure 3 b) which given the pairwise particle states p_i and p_j , their relation r_{ij} , and input effects e_i^0 , outputs the total propagated effect e_i on each particle p_i .

State Prediction Module We use a simple fully-connected network ψ to predict the next particle states P^{t+1} . In order to get more accurate predictions, we leverage the hierarchical particle representation by predicting the dynamics of any given particle within the local coordinate system originated at its parent. The only exceptions are object root particles for which we predict the global dynamics. Specifically, the *state prediction module* $\psi(g, p_i, e_i)$ predicts the local future delta position $\delta_{i,\ell}^{t+1} = \delta_i^{t+1} - \delta_{\text{par}(i)}^{t+1}$ using the particle state p_i , the total effect e_i on p_i , and the gravity g as input. The final future delta position in world coordinates is computed from local information as $\delta_i^{t+1} = \delta_{i,\ell}^{t+1} + \sum_j \delta_{j,\ell}^{t+1}, j \in \text{anc}(i)$.

4.3 Learning Physical Constraints through Loss Functions and Data

Traditionally, physical systems are modeled with equations providing fixed approximations of the real world. Instead, we choose to learn physical constraints, including the meaning of the material property vector, from data. The error signal we found to work best is a combination of three objectives. (1) We predict the position change $\delta_{i,\ell}^{t+1}$ between time step t and $t + 1$ independently for all particles in the hierarchy. In practice, we find that $\delta_{i,\ell}^{t+1}$ will differ in magnitude for particles in different levels. Therefore, we normalize the local dynamics using the statistics from all particles in the same level (*local loss*). (2) We also require that the global future delta position δ_i^{t+1} is accurate, which is computed by combining the predicted local deltas as $\delta_i^{t+1} = \delta_{i,\ell}^{t+1} + \sum_j \delta_{j,\ell}^{t+1}, j \in \text{anc}(i)$ (*global loss*). (3) We aim to preserve the intra-object particle structure by imposing that the pairwise distance between two connected particles p_i and p_j in the next time step $d^{t+1}(i, j)$ matches the ground truth. In the case of a rigid body this term works to preserve the distance between particles. For soft bodies, this objective ensures that pairwise local deformations are learned correctly (*preservation loss*).

The total objective function linearly combines (1), (2), and (3) weighted by hyperparameters α and β :

$$\text{Loss} = \alpha \left(\sum_{p_i} \|\hat{\delta}_{i,\ell}^{t+1} - \delta_{i,\ell}^{t+1}\|^2 + \beta \sum_{p_i} \|\hat{\delta}_i^{t+1} - \delta_i^{t+1}\|^2 \right) + (1 - \alpha) \sum_{p_i \in \text{sib}(p_j)} \|\hat{d}^{t+1}(i, j) - d^{t+1}(i, j)\|^2$$

5 Experiments

In this section, we examine the HRN’s ability to accurately predict the physical state across time in scenarios with rigid bodies, deformable bodies, collisions and external actions. We also evaluate the generalization performance across various object and environment properties. Finally, we present some more complex scenarios including (e.g.) falling block towers and dominoes. We strongly encourage readers to have a look at result examples shown in main text figures, supplementary materials, and at <https://youtu.be/DDHLM6bU8g>.

All training data for the below experiments was generated via a custom *interactive particle-based environment* based on the FleX physics engine [30] in Unity3D. This environment provides (1) an automated way to extract a particle representation given a 3D object mesh, (2) a convenient way to generate randomized physics scenes for generating static training data, and (3) a standardized way to interact with objects in the environment through forces. Code for this environment, along with the entire HRN code base, will be released in the near future.

5.1 Qualitative evaluation of physical phenomena

Rigid body kinematic motion, external forces and collisions. In a first experiment, rigid objects are pushed up, via an externally applied force, from a ground plane then fall back down and collide with the plane. The model is trained on 10 different shapes (cube, sphere, pyramid, cylinder, cuboid, torus, prism, octahedron, ellipsoid, flat deformed pyramid) with 50-300 particles each. The static plane is represented using 5,000 particles with a practically infinite mass. Initial external impulses are spatially dispersed with a Gaussian kernel on particles applied at randomly chosen points on

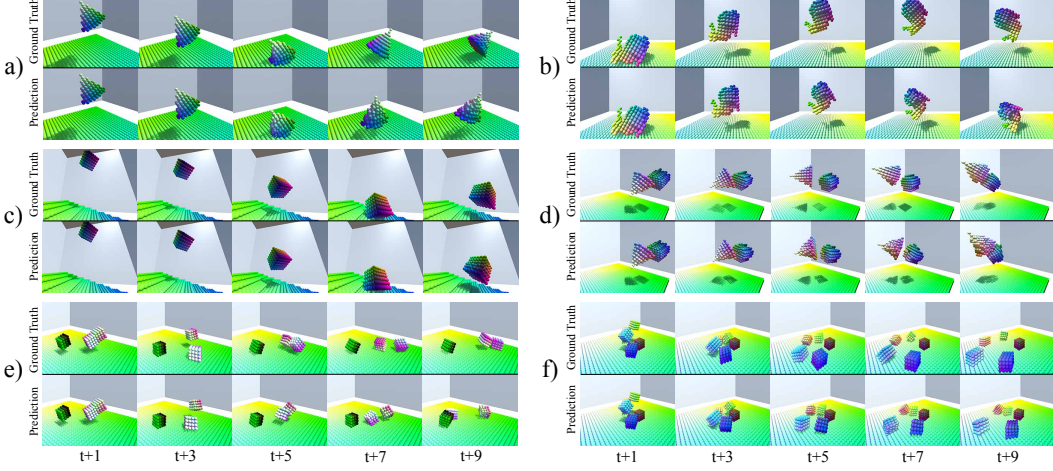


Figure 5: **Prediction examples and ground truth.** **a)** A cone bouncing off a plane. **b)** Parabolic motion of a bunny. A force is applied at the first frame. **c)** A cube falling on a slope. **d)** A cone colliding with a pentagonal prism. Both shapes were held-out. **e)** Three objects colliding on a plane. **f)** Falling block tower not trained on. We strongly recommend watching the videos in the supplement.

the object surface. Testing is performed on instances of the same rigid shapes, but with new forces and application points. Results can be seen in supplementary Figure E.7 c) and d), illustrating that the HRN correctly predicts the parabolic kinematic trajectories of tangentially accelerated objects, rotation due to torque, responses to initial external impulses, and the eventual elastic collisions of the object with the floor.

Complex shapes. To show that our model also extends to complex non-convex shapes (e.g. bunny, duck, teddy, torus), we train and test on such objects colliding with a plane. Figure 5 b) shows an example prediction for the bunny; more examples are shown in supplementary Figure E.7 g) and h).

Deformable bodies. We repeat the same experiment but with deformable bodies of varying stiffness, showing that HRN properly handles kinematics, external forces and collisions involving soft bodies. One illustrative result is depicted in Figure 1, showing a non-rigid cube as it deformably bounces off the floor. Additional examples are shown in supplementary Figure E.7 g) and h).

Shape generalization. To illustrate HRN’s generalization capacity, we evaluate testing performance on shapes not seen in training. Shape generalization tests were performed on unseen rigid and non-rigid, simple and complex shapes (e.g. cone, pentagonal prism, bunny) for models trained on a set of different rigid and non-rigid shapes. One result example is shown in Figure 5 a).

Complex surfaces. Since the floor is a physical object, it should be able to take on complex configurations. We examine spheres, cubes, and cylinders falling and then moving along 5 complex surfaces, including slopes, stairs, half-pipes, bowls and a “random” bumpy surface. See Figure 5 c) and supplementary Figure E.8 c), d), and e) for results.

Collisions between moving objects. Collisions between two moving objects are more complicated to predict than static collisions. We first evaluate this setup in a zero-gravity environment to obtain pure collisions. Training was performed with the same 10 shapes from the first experiment. Figure 5 d) shows predictions for collisions involving shapes not seen during training. Additional examples can be found in supplementary Figure E.7 e) and f).

Multi-object interaction. Complex scenarios include simultaneous interactions between multiple moving objects supported by static surfaces. For example when three objects collide on a plane surface, the model has to resolve direct object collisions, indirect collisions through intermediate objects, and forces exerted by the surface to support the objects. To illustrate the HRN’s ability to handle such scenarios, we train on combinations of two and three objects (cube, stick, sphere, ellipsoid, triangular prism, cuboid, torus, pyramid) colliding simultaneously on a plane. See Figure 5 e) and supplementary Figure E.8 f) for results.

Held-out complex scenarios. We also show that HRN trained on the two and three object collision data generalizes to complex new scenarios. Generalization tests were performed on a falling block tower, a falling domino chain and a bowl containing multiple spheres. All setups consist of 5 objects. See Figure 5 f) and supplementary Figures E.7 b) and E.8 b) and g) for results. Although predictions sometimes differ from ground truth in their details, results still appear plausible to human observers.

Response to parameter variation. To evaluate how the HRN responds to changes in mass, gravity and stiffness, we train on datasets in which these properties vary. During testing time we vary those parameters for the same initial starting state and evaluate how trajectories change. In supplementary Figures E.11, E.10 and E.9 we show results for each variation, illustrating e.g. how heavier objects with greater momentum affect trajectories of lighter objects.

Object graph manipulations. We make use of the hierarchical particle graph representation to construct objects that contain both rigid and soft parts. Supplementary Figure E.8 h) shows a half-rigid half-soft pyramid. Although not shown, in theory, one could also simulate shattering objects by removing enough relations between particles within an object. These manipulations are of substantial interest because they go beyond what is possible to generate in our simulation environment.

5.2 Quantitative evaluation and ablation

We compare HRN to several baselines and model ablations. The first baseline is a simple Multi-Layer-Perceptron (MLP) which takes the full particle representation and directly outputs the next particle states. The second baseline is the Interaction Network as defined by Battaglia et al. [4] denoted as *fully-connected graph* as it corresponds to removing our hierarchy and computing on a fully-connected graph. In addition, to show the importance of the ϕ_C , ϕ_F , and ϕ_H modules, we remove and replace them with simple alternatives. *No ϕ_F* replaces the force module by concatenating the forces to the particle states and directly feeding them into η . Similarly for *no ϕ_C* , ϕ_C is removed by adding the collision relations to the object relations and feeding them directly through η . In case of *no ϕ_H* , ϕ_H is simply removed and not replaced with anything. Next, we show that two input time steps ($t, t-1$) improve results by comparing it with a *1 time step* model. Lastly, we evaluate the importance of the *preservation loss* and the *global loss* component added to the *local loss*. An additional evaluation of different grouping methods can be found in Section B of the supplement.

Comparison metrics are the cumulative mean squared error of the absolute global position, position delta, and preserve distance error up to time step $t+9$. Results are reported in Figure 6. The HRN outperforms all controls. The hierarchy is especially important, with the *fully connected graph* and *MLP* baselines performing substantially worse. In qualitative evaluations, we found that using more than one input time step improves results especially during collisions as the acceleration is better estimated which the metrics in Figure 6 confirm. We also found that splitting collisions, forces, history and effect propagation into separate modules with separate weights allows each module to specialize, improving predictions. Lastly, the proposed loss structure is crucial to model training. Without distance preservation or the global delta position prediction our model performs much worse.

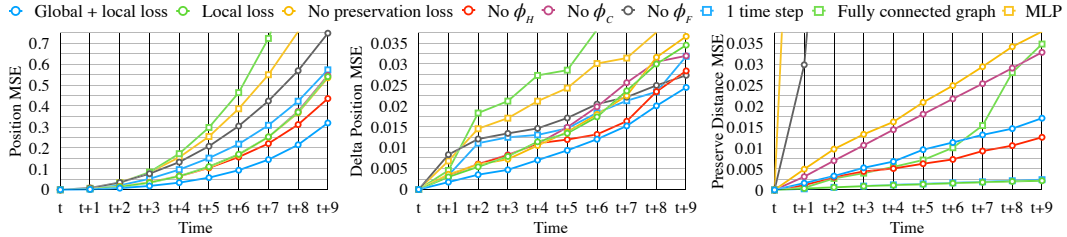


Figure 6: Quantitative evaluation. We compare the full HRN (*global + local loss*) to several baselines, namely *local loss only*, *no preservation loss*, *no ϕ_H* , *no ϕ_C* , *no ϕ_F* , *1 time step*, *fully connected graph* and a *MLP* baseline. The line graphs from left to right show the mean squared error (MSE) between positions, delta positions and distance preservation accumulated over time. Our model has the lowest position and delta position error and a only slightly higher preservation error.

6 Conclusion

We have described a hierarchical graph-based scene representation that allows the scalable specification of arbitrary geometrical shapes and a wide variety of material properties. Using this representation, we introduced a learnable neural network based on hierarchical graph convolution that generates plausible trajectories for complex physical interactions over extended time horizons, generalizing well across shapes, masses, external and internal forces as well as material properties. Because of the particle-based nature of our representation, it naturally captures object permanence identified in cognitive science as a key feature of human object perception [41].

A wide variety of applications of this work are possible. Several of interest include developing predictive models for grasping of rigid and soft objects in robotics, and modeling the physics of 3D point cloud scans for video games or other simulations. To enable a pixel-based end-to-end trainable version of the HRN for use in key computer vision applications, it will be critical to combine our work with adaptations of existing methods (e.g. [52, 22]) for inferring initial (non-hierarchical) scene graphs from image or video data. In the future we also plan to remedy some of HRN’s limitations, expanding the classes of materials it can handle to including cloths, liquids or gases, and to dynamical scenarios in which objects can shatter or merge. This should involve a more sophisticated representation of material properties as well as a more nuanced hierarchical construction. Finally, it will be of great interest to evaluate to what extent HRN-type models describe patterns of human intuitive physical knowledge observed by cognitive scientists [31, 34].

Acknowledgments

We thank Viktor Reutskyy, Miles Macklin, Mike Skolones and Rev Lebaredian for helpful discussions and their support with integrating NVIDIA FleX into our simulation environment. This work was supported by grants from the James S. McDonnell Foundation, Simons Foundation, and Sloan Foundation (DLKY), a Berry Foundation postdoctoral fellowship (NH), and the NVIDIA Corporation.

References

- [1] P. Agrawal, A. V. Nair, P. Abbeel, J. Malik, and S. Levine. Learning to poke by poking: Experiential learning of intuitive physics. In *Advances in Neural Information Processing Systems*, pages 5074–5082, 2016.
- [2] D. Baraff. Physically based modeling: Rigid body simulation. *SIGGRAPH Course Notes, ACM SIGGRAPH*, 2(1):2–1, 2001.
- [3] C. Bates, P. Battaglia, I. Yildirim, and J. B. Tenenbaum. Humans predict liquid dynamics using probabilistic simulation. In *CogSci*, 2015.
- [4] P. Battaglia, R. Pascanu, M. Lai, D. Jimenez Rezende, and k. kavukcuoglu. Interaction networks for learning about objects, relations and physics. In *Advances in Neural Information Processing Systems 29*, pages 4502–4510. 2016.
- [5] P. W. Battaglia, J. B. Hamrick, and J. B. Tenenbaum. Simulation as an engine of physical scene understanding. *Proceedings of the National Academy of Sciences*, 110(45):18327–18332, 2013.
- [6] J. Bender, M. Müller, and M. Macklin. Position-based simulation methods in computer graphics. In *Eurographics (Tutorials)*, 2015.
- [7] M. Brand. Physics-based visual understanding. *Computer Vision and Image Understanding*, 65 (2):192–205, 1997.
- [8] M. M. Bronstein, J. Bruna, Y. LeCun, A. Szlam, and P. Vandergheynst. Geometric deep learning: going beyond euclidean data. *IEEE Signal Processing Magazine*, 34(4):18–42, 2017.
- [9] J. Bruna, W. Zaremba, A. Szlam, and Y. LeCun. Spectral networks and locally connected networks on graphs. *arXiv preprint arXiv:1312.6203*, 2013.
- [10] A. Byravan and D. Fox. Se3-nets: Learning rigid body motion using deep neural networks. In *Robotics and Automation (ICRA), 2017 IEEE International Conference on*, pages 173–180. IEEE, 2017.

- [11] M. B. Chang, T. Ullman, A. Torralba, and J. B. Tenenbaum. A compositional object-based approach to learning physical dynamics. *arXiv preprint arXiv:1612.00341*, 2016.
- [12] E. Coumans. Bullet physics engine. *Open Source Software: http://bulletphysics. org*, 1:3, 2010.
- [13] M. Defferrard, X. Bresson, and P. Vandergheynst. Convolutional neural networks on graphs with fast localized spectral filtering. In *Advances in Neural Information Processing Systems*, pages 3844–3852, 2016.
- [14] D. K. Duvenaud, D. Maclaurin, J. Iparraguirre, R. Bombarell, T. Hirzel, A. Aspuru-Guzik, and R. P. Adams. Convolutional networks on graphs for learning molecular fingerprints. In *Advances in neural information processing systems*, pages 2224–2232, 2015.
- [15] C. Finn, I. Goodfellow, and S. Levine. Unsupervised learning for physical interaction through video prediction. In *Advances in neural information processing systems*, pages 64–72, 2016.
- [16] K. Fragiadaki, P. Agrawal, S. Levine, and J. Malik. Learning visual predictive models of physics for playing billiards. *arXiv preprint arXiv:1511.07404*, 2015.
- [17] R. Grzeszczuk, D. Terzopoulos, and G. Hinton. Neuroanimator: Fast neural network emulation and control of physics-based models. In *Proceedings of the 25th annual conference on Computer graphics and interactive techniques*, pages 9–20. ACM, 1998.
- [18] N. Haber, D. Mrowca, L. Fei-Fei, and D. L. Yamins. Learning to play with intrinsically-motivated self-aware agents. *arXiv preprint arXiv:1802.07442*, 2018.
- [19] J. Hamrick, P. Battaglia, and J. B. Tenenbaum. Internal physics models guide probabilistic judgments about object dynamics. In *Proceedings of the 33rd annual conference of the cognitive science society*, pages 1545–1550. Cognitive Science Society Austin, TX, 2011.
- [20] M. Hegarty. Mechanical reasoning by mental simulation. *Trends in cognitive sciences*, 8(6):280–285, 2004.
- [21] M. Henaff, J. Bruna, and Y. LeCun. Deep convolutional networks on graph-structured data. *arXiv preprint arXiv:1506.05163*, 2015.
- [22] T. Kipf, E. Fetaya, K.-C. Wang, M. Welling, and R. Zemel. Neural relational inference for interacting systems. *arXiv preprint arXiv:1802.04687*, 2018.
- [23] T. N. Kipf and M. Welling. Semi-supervised classification with graph convolutional networks. *arXiv preprint arXiv:1609.02907*, 2016.
- [24] T. D. Kulkarni, V. K. Mansinghka, P. Kohli, and J. B. Tenenbaum. Inverse graphics with probabilistic cad models. *arXiv preprint arXiv:1407.1339*, 2014.
- [25] T. D. Kulkarni, W. F. Whitney, P. Kohli, and J. Tenenbaum. Deep convolutional inverse graphics network. In *Advances in Neural Information Processing Systems*, pages 2539–2547, 2015.
- [26] B. M. Lake, T. D. Ullman, J. B. Tenenbaum, and S. J. Gershman. Building machines that learn and think like people. *Behavioral and Brain Sciences*, 40, 2017.
- [27] A. Lerer, S. Gross, and R. Fergus. Learning physical intuition of block towers by example. *arXiv preprint arXiv:1603.01312*, 2016.
- [28] W. Li, S. Azimi, A. Leonardis, and M. Fritz. To fall or not to fall: A visual approach to physical stability prediction. *arXiv preprint arXiv:1604.00066*, 2016.
- [29] Y. Li, D. Tarlow, M. Brockschmidt, and R. Zemel. Gated graph sequence neural networks. *arXiv preprint arXiv:1511.05493*, 2015.
- [30] M. Macklin, M. Müller, N. Chentanez, and T.-Y. Kim. Unified particle physics for real-time applications. *ACM Transactions on Graphics (TOG)*, 33(4):153, 2014.
- [31] M. McCloskey, A. Caramazza, and B. Green. Curvilinear motion in the absence of external forces: Naive beliefs about the motion of objects. *Science*, 210(4474):1139–1141, 1980.

[32] R. Mottaghi, H. Bagherinezhad, M. Rastegari, and A. Farhadi. Newtonian scene understanding: Unfolding the dynamics of objects in static images. In *Proceedings of the IEEE Conference on Computer Vision and Pattern Recognition*, pages 3521–3529, 2016.

[33] R. Mottaghi, M. Rastegari, A. Gupta, and A. Farhadi. “what happens if...” learning to predict the effect of forces in images. In *European Conference on Computer Vision*, pages 269–285. Springer, 2016.

[34] L. Piloto, A. Weinstein, A. Ahuja, M. Mirza, G. Wayne, D. Amos, C.-c. Hung, and M. Botvinick. Probing physics knowledge using tools from developmental psychology. *arXiv preprint arXiv:1804.01128*, 2018.

[35] C. R. Qi, H. Su, K. Mo, and L. J. Guibas. Pointnet: Deep learning on point sets for 3d classification and segmentation. *Proc. Computer Vision and Pattern Recognition (CVPR), IEEE*, 1(2):4, 2017.

[36] C. R. Qi, L. Yi, H. Su, and L. J. Guibas. Pointnet++: Deep hierarchical feature learning on point sets in a metric space. In *Advances in Neural Information Processing Systems*, pages 5105–5114, 2017.

[37] F. Scarselli, M. Gori, A. C. Tsoi, M. Hagenbuchner, and G. Monfardini. The graph neural network model. *IEEE Transactions on Neural Networks*, 20(1):61–80, 2009.

[38] M. Schlichtkrull, T. N. Kipf, P. Bloem, R. v. d. Berg, I. Titov, and M. Welling. Modeling relational data with graph convolutional networks. *arXiv preprint arXiv:1703.06103*, 2017.

[39] K. A. Smith and E. Vul. Sources of uncertainty in intuitive physics. *Topics in cognitive science*, 5(1):185–199, 2013.

[40] E. S. Spelke. Principles of object perception. *Cognitive science*, 14(1):29–56, 1990.

[41] E. S. Spelke, K. Breinlinger, J. Macomber, and K. Jacobson. Origins of knowledge. *Psychological review*, 99(4):605, 1992.

[42] I. Sutskever and G. E. Hinton. Using matrices to model symbolic relationship. In *Advances in Neural Information Processing Systems*, pages 1593–1600, 2009.

[43] J. B. Tenenbaum, C. Kemp, T. L. Griffiths, and N. D. Goodman. How to grow a mind: Statistics, structure, and abstraction. *science*, 331(6022):1279–1285, 2011.

[44] D. Tran, L. Bourdev, R. Fergus, L. Torresani, and M. Paluri. Learning spatiotemporal features with 3d convolutional networks. In *Computer Vision (ICCV), 2015 IEEE International Conference on*, pages 4489–4497. IEEE, 2015.

[45] D. Tran, L. Bourdev, R. Fergus, L. Torresani, and M. Paluri. Deep end2end voxel2voxel prediction. In *Computer Vision and Pattern Recognition Workshops (CVPRW), 2016 IEEE Conference on*, pages 402–409. IEEE, 2016.

[46] T. Ullman, A. Stuhlmüller, N. Goodman, and J. B. Tenenbaum. Learning physics from dynamical scenes. In *Proceedings of the 36th Annual Conference of the Cognitive Science society*, pages 1640–1645, 2014.

[47] Z. Wang, S. Rosa, B. Yang, S. Wang, N. Trigoni, and A. Markham. 3d-physnet: Learning the intuitive physics of non-rigid object deformations. *arXiv preprint arXiv:1805.00328*, 2018.

[48] N. Watters, A. Tacchetti, T. Weber, R. Pascanu, P. Battaglia, and D. Zoran. Visual interaction networks. *arXiv preprint arXiv:1706.01433*, 2017.

[49] W. F. Whitney, M. Chang, T. Kulkarni, and J. B. Tenenbaum. Understanding visual concepts with continuation learning. *arXiv preprint arXiv:1602.06822*, 2016.

[50] J. Wu, I. Yildirim, J. J. Lim, B. Freeman, and J. Tenenbaum. Galileo: Perceiving physical object properties by integrating a physics engine with deep learning. In *Advances in neural information processing systems*, pages 127–135, 2015.

- [51] J. Wu, J. J. Lim, H. Zhang, J. B. Tenenbaum, and W. T. Freeman. Physics 101: Learning physical object properties from unlabeled videos. In *BMVC*, volume 2, page 7, 2016.
- [52] J. Wu, T. Xue, J. J. Lim, Y. Tian, J. B. Tenenbaum, A. Torralba, and W. T. Freeman. Single image 3d interpreter network. In *European Conference on Computer Vision*, pages 365–382. Springer, 2016.

Supplementary Material

A Iterative hierarchical grouping algorithm

We describe the iterative grouping algorithm used to generate our hierarchical particle-based object representation in Algorithm 1:

Algorithm 1: Iterative hierarchical grouping algorithm.

input : Scene graph $G = \langle P, R \rangle$ with particles P and relations R and target cluster size N_C
output : Hierarchical scene graph $G_H = \langle P_H, R_H \rangle$
begin

Initialize $R_H = \{\}$ and $P_H = \{\}$;

for connected component (object) $o \in G$ **do**

Initialize $R_o = \{\}$ and $P_o = \{p_i | i \in o\}$;

Create root particle $p_{\text{root}} = \langle \frac{1}{|P_o|} \sum_{i \in o} x_i, \frac{1}{|P_o|} \sum_{i \in o} \delta_i, \sum_{i \in o} m_i \rangle$;

Connect p_{root} to leaves(p_{root}) with relations $R_{\text{A2D}} \equiv \{r_{ij} | i = \text{root}; p_j \in \text{leaves}(p_{\text{root}})\}$;

Connect leaves(p_{root}) to p_{root} with relations $R_{\text{L2A}} \equiv \{r_{ij} | p_i \in \text{leaves}(p_{\text{root}}); j = \text{root}\}$;

Add relations to $R_o \equiv R_o \cup R_{\text{A2D}} \cup R_{\text{L2A}}$;

Initialize the particle processing queue $q = \{p_{\text{root}}\}$;

while q not empty **do**

Get current particle $p_{\text{curr}} = \text{pop}(q)$;

Initialize processed subcomponent indexes $I_s = \{\}$;

if $|\text{leaves}(p_{\text{curr}})| \geq N_C$ **then**

Use k-means to group leaves(p_{curr}) into N_C subcomponents $\{S_1, S_2, \dots, S_{N_C}\}$;

for subcomponent $S \in \{S_1, S_2, \dots, S_{N_C}\}$ **do**

if $|S| > 1$ **then**

Create new root particle for subcomponent $p_s = \langle \frac{1}{|S|} \sum_{i \in S} x_i, \frac{1}{|S|} \sum_{i \in S} \delta_i, \sum_{i \in S} m_i \rangle$;

Connect all anc(p_s) to p_s with relations $R_{\text{A2D}}^1 \equiv \{r_{is} | p_i \in \text{anc}(p_s)\}$;

Connect p_s to all leaves(p_s) with relations $R_{\text{A2D}}^2 \equiv \{r_{sj} | p_j \in \text{leaves}(p_s)\}$;

Connect all leaves(p_s) to p_s with relations $R_{\text{L2A}} \equiv \{r_{is} | p_i \in \text{leaves}(p_s)\}$;

Add relations to $R_o \equiv R_o \cup R_{\text{A2D}}^1 \cup R_{\text{A2D}}^2 \cup R_{\text{L2A}}$;

Add p_s to $P_o \equiv P_o \cup \{p_s\}$;

Add S to $I_s \equiv I_s \cup \{S\}$;

Append p_s to processing queue $q = \text{push}(p_s, q)$;

end

else

Add S to $I_s \equiv I_s \cup S$;

end

end

end

end

else

Set $I_s \equiv \{i | p_i \in \text{leaves}(p_{\text{curr}})\}$;

end

Connect all particle pairs p_i and p_j in I_s with $R_{\text{WS}} \equiv \{r_{ij} | i, j \in I_s\}$;

Add R_{WS} to $R_o \equiv R_o \cup R_{\text{WS}}$;

end

Add relations R_o to $R_H \equiv R_H \cup R_o$;

Add particles P_o to $P_H \equiv P_H \cup P_o$;

end

Return $G_H = \langle P_H, R_H \rangle$;

end

B Comparison of different grouping methods

While performing a hyperparameter search we also tried several different grouping methods. Here, we compare agglomerative clustering against different versions of k-means. Specifically, we tried to generate hierarchies with up to 8 particles and 10 particles per group grouped by k-means. As seen in Figure B.1 and Figure B.2 we found that k-means with 8 particle groups works best resulting in a reasonable trade-off between number of particles per group and number of hierarchical layers for the tested objects. However, the improvement over the other clustering algorithms is minor, indicating that HRN is robust to the grouping method.

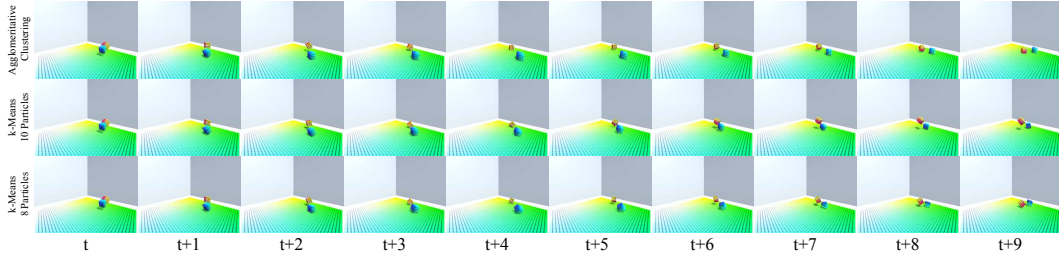


Figure B.1: **Qualitative comparison of different grouping methods.** Agglomerative grouping (top) is compared against k-means with up to 10 particles per group (middle), and k-means with up to 8 particles per group (bottom) which is used in HRN.

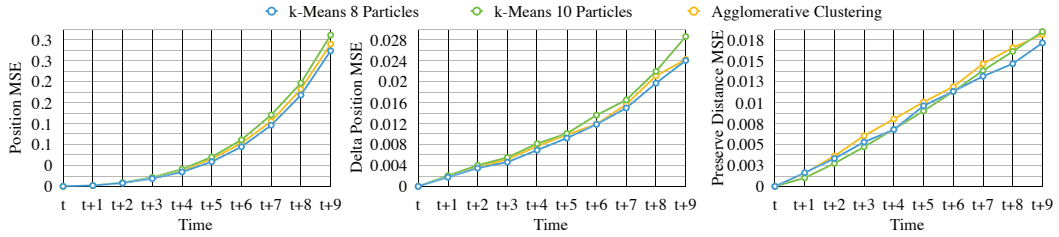


Figure B.2: **Quantitative comparison of different grouping methods.** Agglomerative grouping (yellow) is compared against k-means with up to 10 particles per group (green), and k-means with up to 8 particles per group (blue) which is used in HRN.

C Implementation details

C.1 Detailed model structure

The HRN is given the states $P_o^{(t-T, t]}$, the gravity g and any external forces F . It is trained to predict the future particle states P_o^{t+1} for each object o . In our implementation, the model actually predicts the change in position $\Delta^{t+1} \equiv X^{t+1} - X^t$, and use Δ^{t+1} to advance the particle states. Note that $X_o^t \equiv \{x_j^t | p_j \in P_o\}$ is the set of all particle positions in o .

Figure C.3 shows a detailed overview of HRN model architecture. In total, there are five modules, each with their own MLP. The dotted box denotes shared weights between the three hierarchical graph convolution stages, η_{L2A} , η_{WS} , and η_{A2D} . All MLPs use a ReLU nonlinearity. The number of units, layers, and output dimension of each MLP were chosen through a hyperparameter search. The gravity input g to Ψ is only added for the global super-particles of each object.

C.2 Training procedure

We train the network using the Adam optimizer with a batch size of 256 across multiple Nvidia Titan Xp GPUs. The initial learning rate was set at 0.001 and decayed stepwise a total of 3 times, alternating between a factor of 2 and 5 each step. We used TensorFlow for the implementation. For the generalization experiments we include data augmentation in the form of random grouping, mass, and translation.

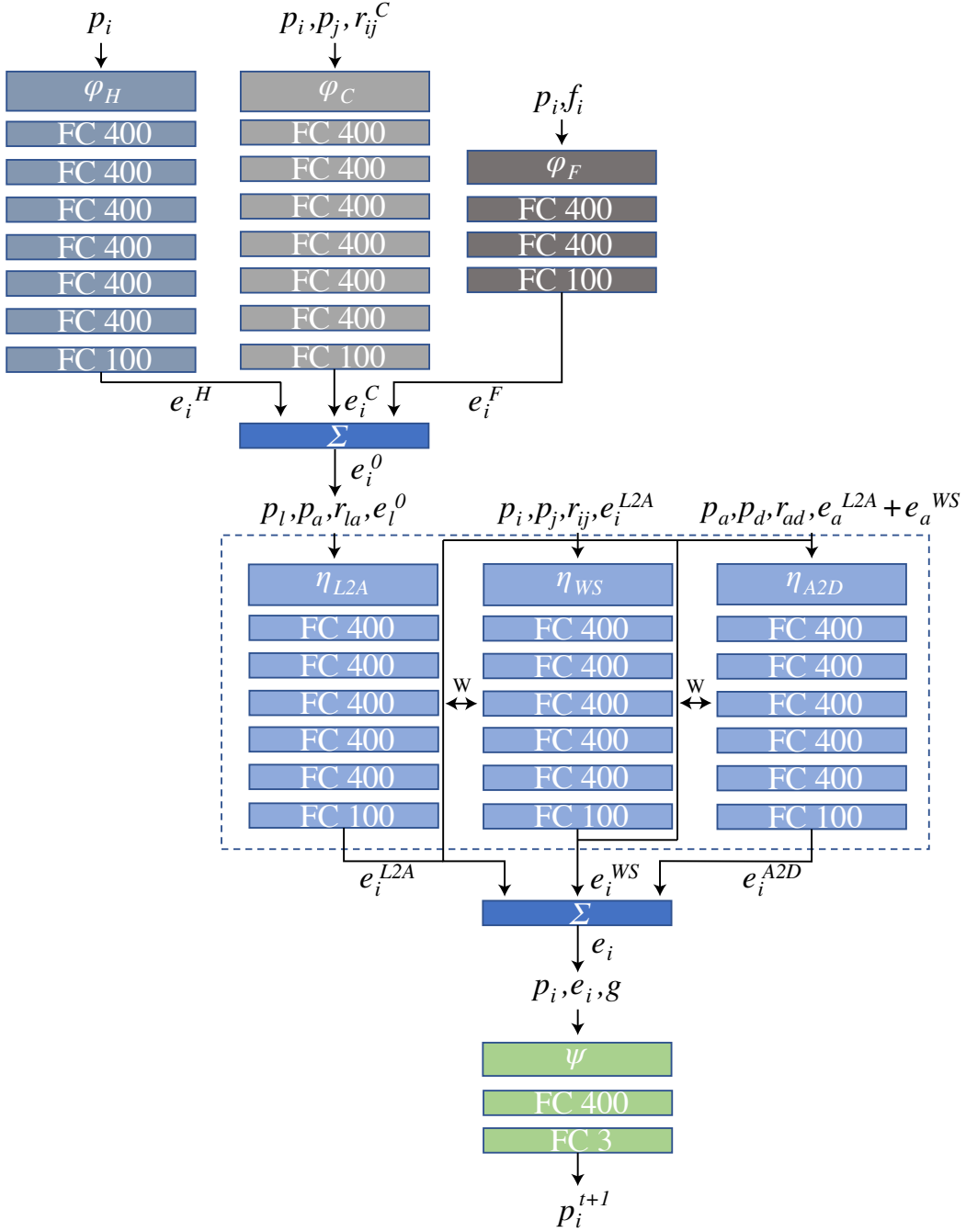


Figure C.3: Detailed description of the HRN model architecture.

D Detailed experimental setups

D.1 Particle-based physics simulation environment

Based on the FleX physics engine [30] we built a custom *interactive particle-based environment* in Unity3D. This environment automatically decomposes any given 3D object mesh into a particle representation using the FleX API. On top of this representation it provides a convenient way to generate randomized physics scenes for generating static training data. The user is able to construct random scenes through a python interface that communicates with Unity3D. This interfaces also

allows for physical interactions with objects within a defined scene. For instance, one can apply forces to a whole object or individual particles to generate translational and rotational position variations. It is both possible to generate static datasets from the environment and to train offline as well as to train and interact with the environment online. Therefore the environment sends the python script client the particle state at every frame as well as images captured by a camera in the scene. Scenes can be rendered with around 30 frames per second. The simulation time increases with the number of particles. Figure D.4 shows a screenshot of the environment embedded in the Unity3D editor. Mesh skins are used to mask the particles in the main scene to give the impression of a continuous object. In the lower right of this screenshot we can see the particle representation of the cube in the scene after FleX has converted the 3D mesh into a particle representation. Code for this environment, along with the entire HRN code base, will be released on acceptance.

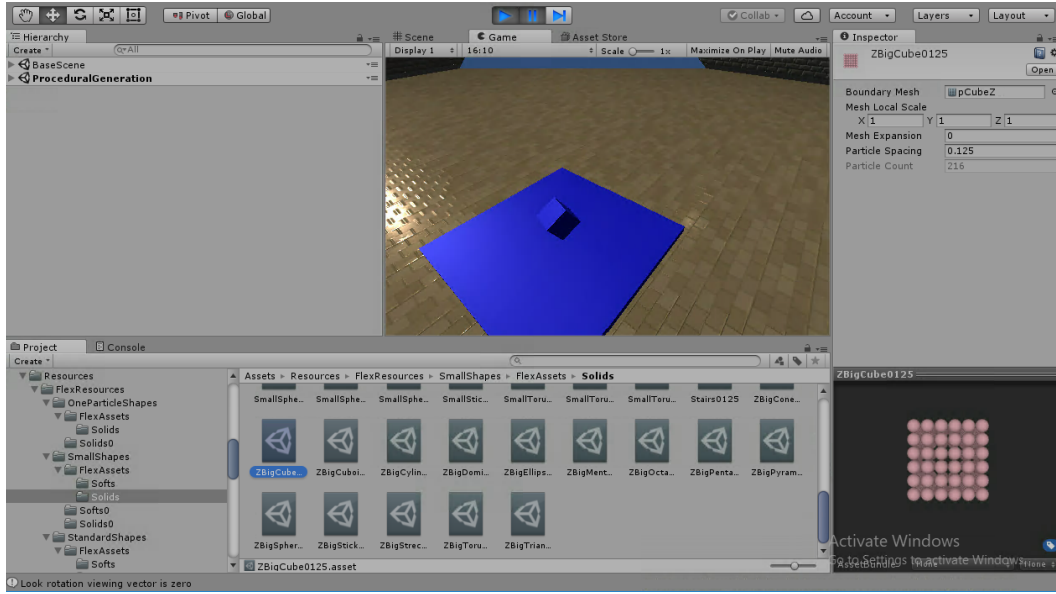


Figure D.4: Particle-based Interaction Environment in Unity3D. Screenshot of the Unity Editor with FleX Plugin. In the main scene a cube is colliding with a planar surface. The lower right shows the particle representation of the cube. This environment is used to generate training and validation data through interactions with objects in the scene. Interactions with the environment are possible through a python interface.

D.2 Shapes and surfaces used during experiments

Figure D.5 and Figure D.6 show the 3D mesh and the leaf particle representation of all shapes and surfaces used during training or testing. Moving objects consist of 50-300 particles, surfaces of more than 5000 particles. Only one particle resolution is shown although multiple levels of detail in the leaf node representation are possible by changing the particle spacing within an object.

D.3 Throwing one object in the air

In this experiment any one of the small shapes depicted in Figure D.5 is first chosen to collide with one of the surfaces in Figure D.6. The small shape is teleported to a random location around the center of the surface. The stiffness is randomly chosen per object after a teleport. As the simulation starts the shape falls on the surface and collides with it. Every random number of frames we apply a randomly upward and perpendicular to the surface pointing force to lift the object up and watch it fall again as it describes a parabola. If the object leaves the surface boundaries we randomly teleport it back to the center. After a fixed number of steps we reinitialize the scene and the whole simulation procedure starts again.

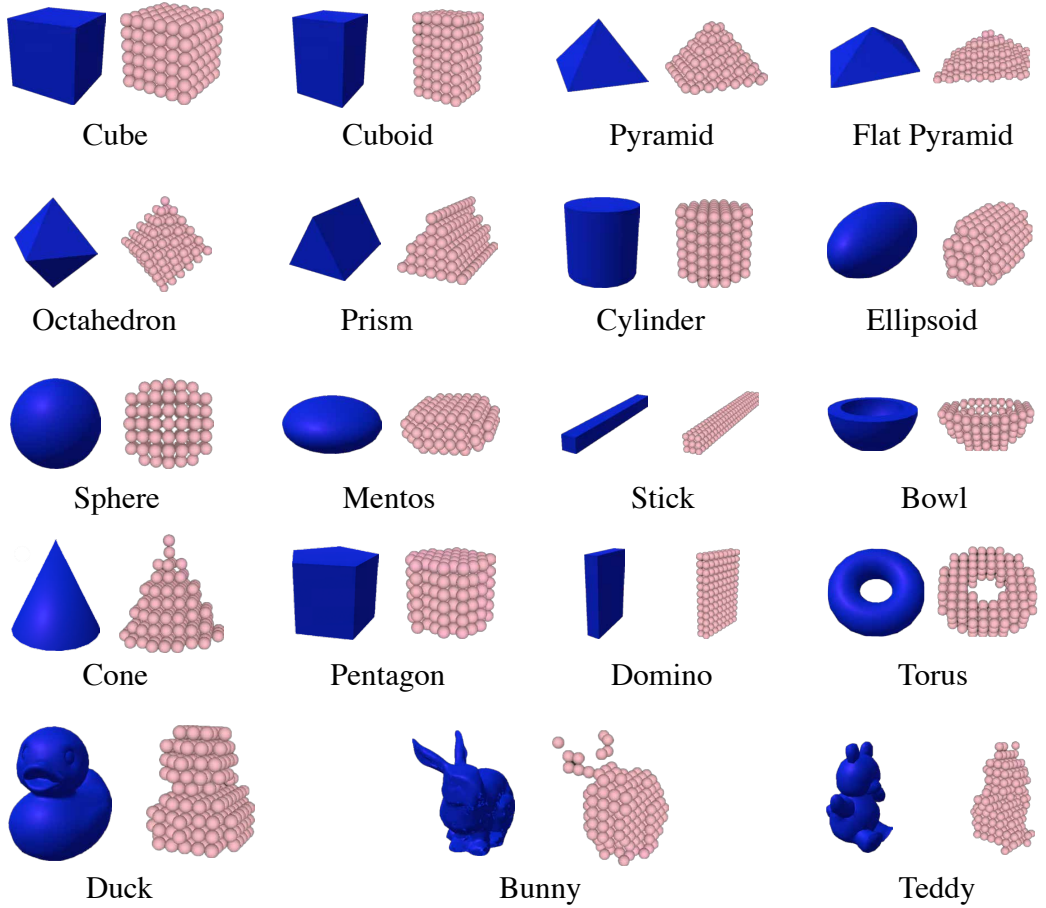


Figure D.5: **Dynamic shapes and particle representations.** All shapes used during testing and training are shown. Shapes consist of 50 - 300 particles. Only one particle resolutions is shown.

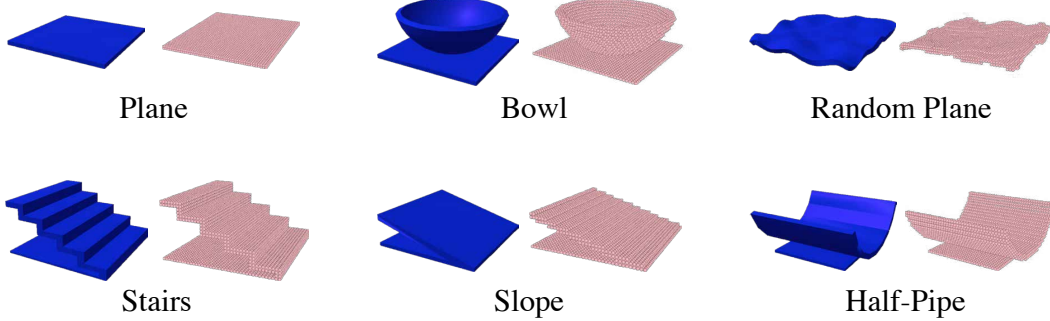


Figure D.6: **Surfaces and particle representations.** All surfaces used during testing and training are shown. Surfaces consist of 5000 - 7000 particles.

D.4 Collisions between objects without gravity

This experimental setup is very similar to *throwing an object in the air* with the difference that gravity is disabled, and we choose two small dynamic shapes that collide with each other in the air. The stiffness is randomly chosen per object after a teleport. Forces are applied such that they either point directly from one object to the other or away from each other. The force magnitude and perturbations to the force direction are randomly chosen every time an action is applied. Forces are

applied randomly either to one or both objects at the same time. The simulation is reinitialized if any of the two objects leaves the room boundaries.

D.5 Collisions between objects on a planar surface

This experiment is a combination of the previous two experiments. Just as in *throwing one object in the air* the two or three chosen small objects are spawned randomly around the center of the planar surface. The stiffness is randomly chosen per object after a teleport. They fall and collide with the plane. Similar to *collisions between objects without gravity* the force is applied such that the two objects collide with each other or are torn apart. The force magnitude and perturbations to the force direction are again randomly chosen. Forces are applied randomly either to one or two objects at the same time. The scene is reinitialized if any of the two objects leaves the surface boundaries.

D.6 Stacked tower

In this experiment we manually construct a tower consisting of 5 stacked rigid cubes on a planar surface. The positions of the cubes are slightly randomly perturbed to create towers of variable stability. After a random number of frames a force is applied to a randomly chosen cube usually big enough to make the tower fall. Once the tower falls and the cubes do not move anymore or after a maximum number of time steps the setup is reset and repeated.

D.7 Dominoes

Similar to the stacked tower, we manually setup a scene in which a rigid dominoes chain is place on top of a planar surface. Small random perturbations are applied to the initial position of each domino. After a random number of frames a force is applied to one or both sides of the chain to make it fall. Once dominoes do not move anymore or after a fixed maximum number of time steps the setup is reset and repeated.

D.8 Balls in bowl

The last manually constructed control example are 5 balls dropping into a big bowl. The spheres are teleported to a randomly chosen position above the bowl. The balls then drop into the ball and interact with each other. A random force is applied every random number of frames. Once the spheres have settled or after a maximum number of time steps we reinitialize the scene.

E Qualitative prediction examples

In the following figures we show additional qualitative examples with different objects and physical setups. We also show more failure cases.

In Figure E.9 we demonstrate the model's ability to handle varying stiffness inputs. The network is trained on multiple soft bodies of varying stiffness. The stiffness values are obtained from FleX during dataset generation and vary between 0.1 and 0.9 for soft bodies. By manually changing the input stiffness during testing, we can produce predictions of objects with varying levels of rigidity. The decreasing level of deformation in frame $t + 5$, from top to bottom, is consistent with the increasing stiffness.

We also test whether the model can capture physical relationships in varying gravitational fields. Since the value of gravity is also an input to our model, we can train on data with changing a changing gravitational constant. Figure E.10 shows an example with four different gravitational constants, ranging from 1 to 20 m/s^2 . As expected, the object falls faster with more gravity.

As part of the particle state, we include the mass of each particle. While the total object mass is usually kept constant for most of the experiments, we test the case of varying mass by training on a dataset where the each object's mass will vary by a factor of up to three times. In Figure E.11 we manually increase the mass of one of the two objects in the collision and show that the heavier object is displaced less after the collision.

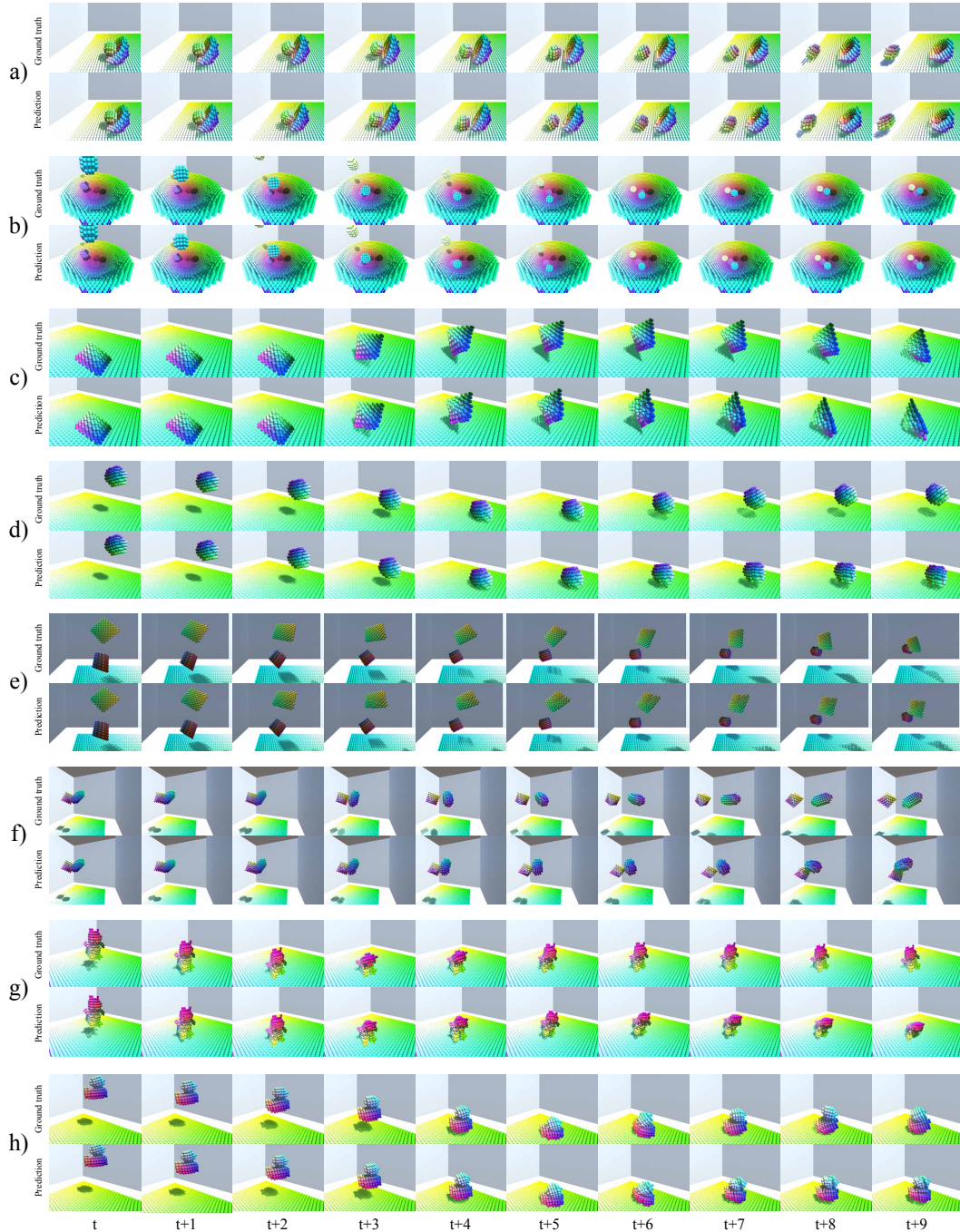


Figure E.7: **Qualitative comparison of HRN predictions vs ground truth.** **a)** A sphere falling out of a bowl. Objects containing other objects can be easily modeled. **b)** Five spheres fall into a ball and collide with each other. Complex indirect collisions occur. **c)** A rigid pyramid colliding with the floor. **d)** A rigid sphere colliding with the floor. **e)** A cylinder colliding with a pyramid. **f)** Ellipsoid and octahedron colliding with each other. **g)** A soft teddy colliding with the floor. **h)** A soft duck colliding with the floor.

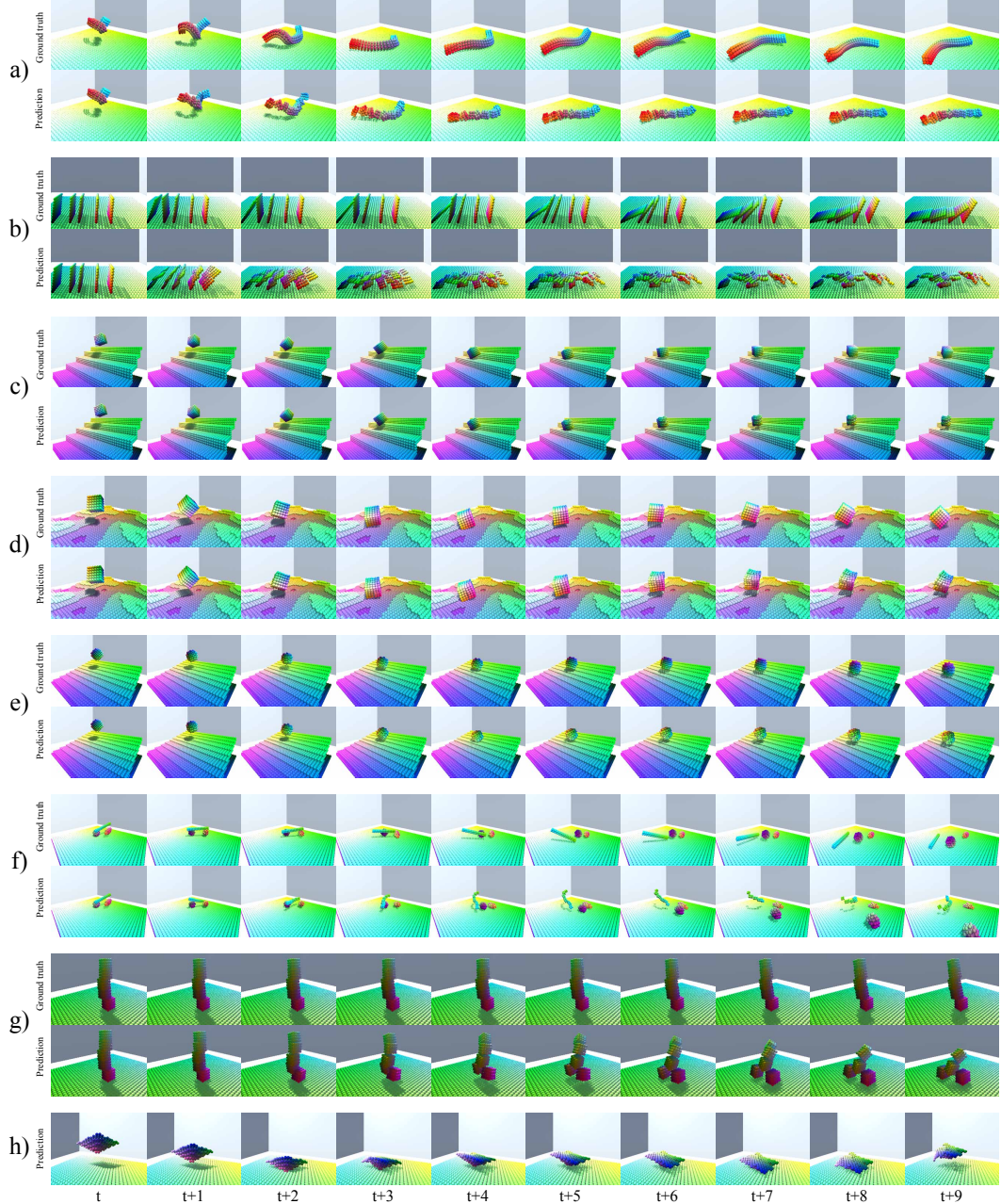


Figure E.8: Qualitative comparison of HRN predictions vs ground truth. **a)** A very deformable stick. The ground truth shape had to be fed into the model for this prediction to work. **b)** Falling dominoes. HRN struggles keeping the shape of the dominoes which could be due to the complex multi-object interactions or the flat nature of a domino. **c)** A rigid cube colliding with stairs. **d)** A cube colliding with a random surface. **e)** A ball on a slope. **f)** Three objects colliding with each other. **g)** A slowly falling tower. The tower in the HRN prediction collapses much faster compared to ground truth. **h)** A half-rigid (right object side) half-soft (left object side) body colliding with a planar surface. The soft part deforms. The rigid part does not deform.

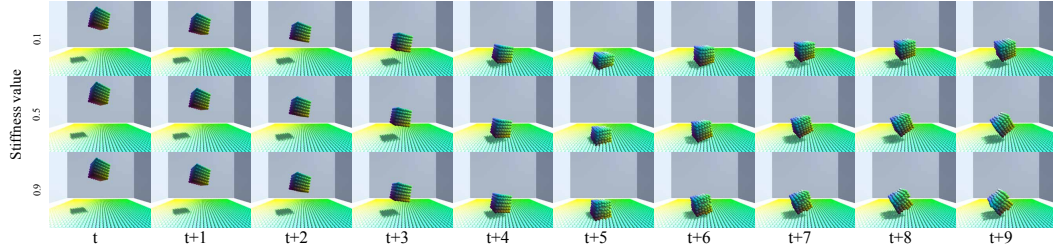


Figure E.9: **Responsiveness to stiffness variations.** We vary the stiffness of a cube colliding with a planar surface. The top row shows a soft cube with stiffness value 0.1, the middle row a stiffness value of 0.5, and the bottom row a almost rigid cube with a stiffness value of 0.9. Our network responds as expected to the changing stiffness value deforming the soft cube stronger than the rigid cube.

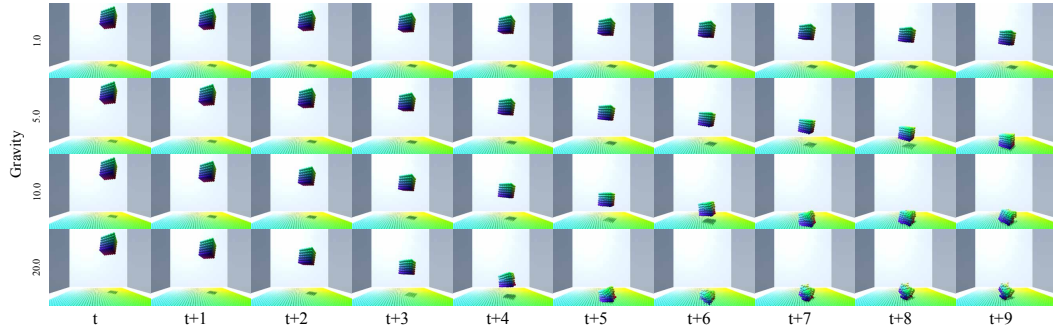


Figure E.10: **Responsiveness to gravity variations.** We vary the gravity while a soft cube is falling on a planar surface. From top to bottom gravity values of 1.0, 5.0, 10.0 and 20.0 m/s^2 are depicted. We can see that the cube falls faster as gravity increases and even deforms the object when colliding with the floor under strong gravity. Our model behaves as expected when gravity changes.

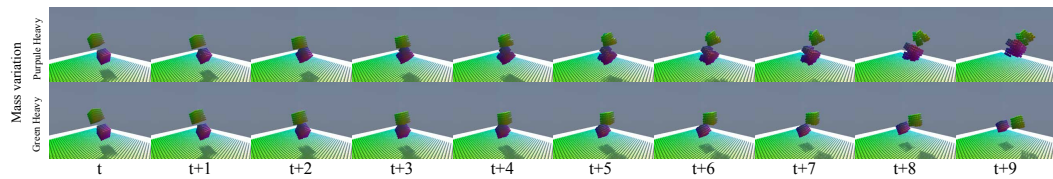


Figure E.11: **Responsiveness to mass variations.** We vary the mass while two cubes collide. The top shows a scenario where the purple cube is heavy. Here the green cube bounces off stronger than the purple one. The bottom shows the same scenario but with green cube being heavy. Here the green cube doesn't move as strongly.